A neighbourhood-scale estimate for the cooling potential of green roofs

Ivo Suter, Čedo Maksimović, Maarten van Reeuwijk

Department of Civil and Environmental Engineering, Imperial College, London, UK
Correspondence to: I. Suter (suter.ivo@bluewin.ch)

November 2016

Abstract. Green roofs offer the possibility to mitigate multiple environmental issues in an urban environment. A common benefit attributed to green roofs is the temperature reduction through evaporation. This study focuses on evaluating the effect that evaporative cooling has on outdoor air temperatures in an urban environment. An established urban energy balance model was modified to quantify the cooling potential of green roofs and study the scalability of this mitigation strategy. Simulations were performed for different climates and urban geometries, with varying soil moisture content, green roof fraction and urban surface layer thickness. All simulations show a linear relationship between surface layer temperature reduction ΔT_s and domain averaged evaporation rates from vegetation mmW, i.e. $\Delta T_\mathrm{s} = e_\mathrm{W} \cdot mmW$, where e_W is the evaporative cooling potential with a value of $\sim -0.35\mathrm{Kday mm}^{-1}$. This relationship is independent of the method by which water is supplied. We also derive a simple algebraic relation for e_W using a Taylor series expansion.

Submitted to: *Urban Climate*

1. Introduction

The fast growth of global population, mainly in urban areas [UNFPA, 2012] and the concurrent increase in likelihood of extreme weather events [IPCC, 2014] forces cities to prepare for water scarcity and heat spells. The fact that cities are several degrees warmer than the surrounding rural environment, known as the urban heat island effect, amplifies this risk [Rosenzweig et al., 2015]. Simultaneously, heavy precipitation and flooding are expected to become more likely in many European cities [Rojas et al., 2012]. As a consequence, the integrated management of water becomes an increasingly important part of urban planning both in terms of flood and urban heat island risk mitigation [Niemczynowicz, 1999].

Green roofs are often discussed as a possible remedy for these problems. The vegetation and soil of green roofs can retain water and delay discharge after rainfall events, thereby reducing the flood risk. Evaporation of the stored water over time leads to lower roof temperatures by converting sensible into latent heat [Getter and Rowe, 2006]. This also lowers indoor temperatures and reduces the energy demand for cooling [Castleton et al., 2010]. The water availability depends on the local climate as well as green roof design. Tools to assess the benefits of such installations are thus needed for better planning urban development. Central questions an urban planner may have are thus 1) how much cooling can be achieved by green roofs given the available amount of water in a city and 2) how much water is required to achieve a certain amount of cooling.

Quantifying the cooling effect of green roofs on outdoor air temperatures is difficult and various studies suggest only a small temperature reduction on street level [Li et al., 2014, Gromke et al., 2015], [Yang et al., 2016]. Roofs with a high albedo, so-called "cool roofs", reflect a larger proportion of solar radiation than conventional roofs and may excel in reducing outdoor temperatures [Mackey et al., 2012, Georgescu et al., 2014, Santamouris, 2014], but they lack the additional benefits for ecology and water management that green roofs provide [Oberndorfer et al., 2007]. Yet, to significantly improve thermal comfort both cool and green roof strategies need to be implemented on a large scale. This also brings up the question how efficiently the implementation of green roofs can be scaled up. Li et al. [2014] and Sun et al. [2016] describe a linear decrease of air temperature with green roof fraction, Mackey et al. [2012] compare temperature reduction to the normalised difference vegetation index (NDVI) from satellite measurements and also find a linear relationship. However, this dependency is not well understood. If this relation holds in general, a fast way of determining the slope coefficient depending on urban characteristics will be of great support for decision makers and urban planners.

This paper establishes a simple relation to estimate the cooling potential of green

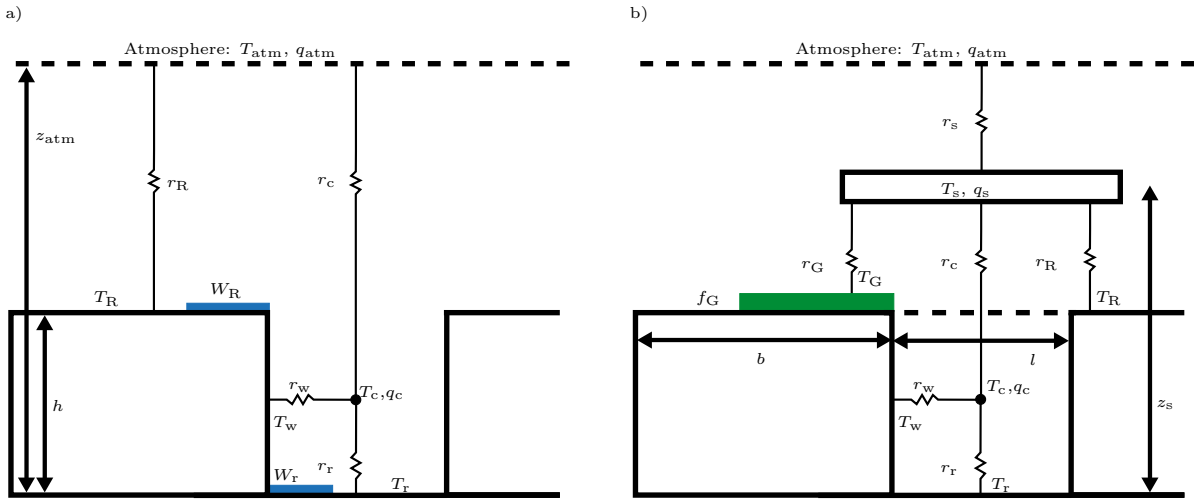

Figure 1. a) Schematic of TEB. b) Schematic of the modified TEB scheme, including the surface layer above the canyon and green roofs. The symbol T denotes temperature, q specific humidity, W water, and r aerodynamic resistance. The subscript $_{\mathrm{R}}$ stands for conventional roof, $_{\mathrm{G}}$ for green roof, $_{\mathrm{r}}$ for road, $_{\mathrm{w}}$ for wall, $_{\mathrm{c}}$ for canyon, $_{\mathrm{s}}$ for surface layer and $_{\mathrm{atm}}$ for the atmosphere. The geometry is given by building height h, building width b and canyon width l. The middle of the surface layer is at an elevation z_s and the atmospheric forcing height is z_{atm}. f_G is the fraction of green roof to total roof area.

roofs for known urban properties and climate. Specifically we 1) quantify the cooling of green roofs on an urban scale taking the urban energy balance (UEB) model approach [Oke, 1988, Grimmond et al., 2010]; 2) examine how the cooling relates to the evaporation rates; and 3) derive a relatively simple equation for the cooling potential for a given amount of water to evaporate. The paper is organised as follows. In section 2 the original UEB model and the changes we made for simulating green roofs in an urban environment are discussed. In section 3 we will present steady and unsteady diurnal cases simulated with the new model and study the effect of surface layer thickness, urban geometry, method of water supply and evaporation from green roofs on the surface layer temperature. In section 4 we derive an algebraic equation to predict the cooling from green roofs and compare it to the findings in section 3. Finally in section 5 we discuss our findings and set them into context of application in real cities.

2. Model description

2.1. Town Energy Budget

The coupling of numerical weather prediction models with the (urban) surface is usually achieved by using land surface modules such as the Town Energy Budget [Masson, 2000, TEB] used by the French national weather service (Météo-France) or the Joint UK Land Environment Simulator [Best et al., 2011, Clark et al., 2011, JULES] by the UK Met

Office. These models are based on a surface energy balance. Urban areas exchange energy in various forms, such as incoming and outgoing longwave ($L^{\downarrow}$, $L^{\uparrow}$) and shortwave radiative fluxes ($S^{\downarrow}$, $S^{\uparrow}$), the turbulent sensible heat flux (H), the turbulent latent heat flux (E), ground heat flux (G) and the net heat storage per unit time ($\Delta Q \equiv dQ/dt$). These fluxes have to balance and the surface energy balance equation is expressed as

$$\Delta Q = (L^{\downarrow} - L^{\uparrow}) + (S^{\downarrow} - S^{\uparrow}) - (H + E + G), \tag{1}$$

where all the terms have unit Wm^{-2}. Additional heat sources could be added if necessary, e.g. anthropogenic heating. UEB models solve a set of ordinary differential equations describing the evolution of heat and water on urban surfaces such as roads, walls and roofs. Air movement is not modelled explicitly; instead aerodynamic resistances are used to describe the turbulent heat and moisture transport in the atmosphere.

We used the open source TEB as starting point for our UEB model. Here we summarise the principles underlying TEB, for a detailed description see Masson [2000]. The urban geometry in TEB is represented as a generic street canyon, including a single conventional roof (R), wall (w) and road (r) surface (figure 1a). The scheme assumes isotropy for the street and house distribution on a large horizontal scale. Equations describing directional process such as radiation are thus integrated horizontally over 360°. TEB therefore does not represent single buildings, but rather the average over a large domain. The canyons are represented by mean building height (h), building width (b) and road width (l). Grimmond et al. [2010] have previously shown that more complex UEB models do not necessarily yield more accurate results. Three distinct energy budgets are considered for the roof, wall and road. The TEB scheme thus takes the form of five coupled differential equations, three for the temperatures and two for the water reservoirs on the roof and the road. The evolution of temperature with time is described as

$$c_{\star} d_{\star} \frac{dT_{\star}}{dt} = S_{\star} + L_{\star} - H_{\star} - E_{\star} - G_{\star}, \tag{2}$$

where $T_{\star}$ [K] represents the roof, wall or road temperature, respectively. The corresponding heat capacity is c [$\mathrm{Jm}^{-3}\mathrm{K}^{-1}$] and the layer thickness d [m]. The water (W) budget on the roof and road is

$$\frac{dW_{\star}}{dt} = P - \frac{E_{\star}}{L_{\mathrm{v}}} - R, \tag{3}$$

where P [$\mathrm{kgm}^{-2}\mathrm{s}^{-1}$] is the precipitation rate, L_{v} [Jkg^{-1}] is the latent heat of vaporization and R is the runoff. The air inside the canyon is assumed not to have any significant heat capacity and therefore its temperature adjusts instantly to the flux balance between road, walls and canyon top. The sensible, latent and ground heat fluxes are defined as, respectively,

$$H_{\star} = \frac{c_{\mathrm{p}} \rho_{\mathrm{a}} (T_{\star} - T_{\mathrm{atm}})}{r_{\star}}, \tag{4}$$

$$E_\star = \frac{L_\mathrm{v}\rho_\mathrm{a}\delta_\star(q_\star - q_\mathrm{atm})}{r_\star}, \tag{5}$$

$$G_\star = \lambda_\star \frac{T_\star - T_\mathrm{bld}}{d_\star}. \tag{6}$$

Here c_p [$\mathrm{Jkg^{-1}K^{-1}}$] is the heat capacity of dry air at constant pressure and ρ_a [$\mathrm{kgm^{-3}}$] is the density of air. The latent heat flux (5) is similar to Eq. (4), where $\delta_\star$ [-] is the fraction of water on the respective surface and q [$\mathrm{kgkg^{-1}}$] is the absolute humidity. Sensible (4) and latent heat fluxes (5) between wall, canyon and atmosphere depend on the aerodynamic resistances $r_\star$ [$\mathrm{sm^{-1}}$]. These resistances describe the transport in the atmosphere and depend on the atmospheric stability, i.e. on the local temperature and wind profile. Ground heat flux (6) is based on one-dimensional thermal conductivity, where $\lambda_\star$ [$\mathrm{Wm^{-1}K^{-1}}$] is the effective thermal conductivity, $d_\star$ [m] is the layer thickness and T_bld [K] is the constant internal building temperature. The walls are described as a single layer with one effective resistance throughout this study. For a complete account of the TEB, especially the treatment of radiation and details on the aerodynamic resistances, see the original model description by Masson [2000].

2.2. Inclusion of green roofs

Since TEB is used as a surface parameterisation for numerical weather prediction models, the fluxes from roof and canyon are directly linked to the atmosphere and they are completely independent of each other (see figure 1a). As a consequence it is not possible to study the effect of roofs on canyon temperature. In order to allow the roof to interact with the other surfaces, it is necessary to introduce an additional air layer between the roof and the atmosphere (figure 1b). The introduction of this surface layer splits the original resistances into two parts. The surface layer air has a moisture content (q_s) and a heat capacity, i.e. temperature (T_s). The evolution of the surface layer's air temperature and absolute humidity are given by

$$c_\mathrm{s} d_\mathrm{s} \frac{dT_\mathrm{s}}{dt} = \left(a_\mathrm{R} H_\mathrm{R} + a_\mathrm{c} H_\mathrm{c} + a_\mathrm{G} H_\mathrm{G} - H_\mathrm{s}\right), \tag{7}$$

$$\rho_\mathrm{a} L_\mathrm{v} d_\mathrm{s} \frac{dq_\mathrm{s}}{dt} = \left(a_\mathrm{R} E_\mathrm{R} + a_\mathrm{c} E_\mathrm{c} + a_\mathrm{G} E_\mathrm{G} - E_\mathrm{s}\right). \tag{8}$$

The fluxes from the canyon, conventional roof, green roof and surface layer are denoted with subscripts $_{\mathrm{c},\mathrm{R},\mathrm{G}}$ and $_\mathrm{s}$, respectively. The flux from the canyon is the sum of the fluxes from the road and the walls. The surface layer stretches the entire area of the urban unit, while the conventional roof, green roof and canyon only cover a part of the area each. The fraction covered by the canyon, green roof and conventional roof are $a_\mathrm{c} = l/(b+l), a_\mathrm{G} = f_\mathrm{G} b/(b+l), a_\mathrm{R} = (1-f_\mathrm{G})b/(b+l)$, respectively. Note that by definition $a_\mathrm{c} + a_\mathrm{G} + a_\mathrm{R} = 1$. The terms in (7) and (8) are thus scaled accordingly. In the context of this study, i.e. during very hot weather, open water surfaces are irrelevant and will not be considered in the remainder of the paper. The green roof temperature

T_{G} is governed by equation (2), whilst the green roof water W_{G}, i.e. soil moisture, is given evolving according to

$$L_v \frac{dW_{\mathrm{G}}}{dt} = L_{\mathrm{v}} P + f_{\mathrm{W}} - E_{\mathrm{G}} - R, \tag{9}$$

where $f_{\mathrm{W}}/L_{\mathrm{v}}$ is the additional supply through watering of the plants in $\mathrm{kgm^{-2}s^{-1}}$. To represent the evaporation from vegetation and soil the Penman-Monteith approach [Jarvis, 1976, Noilhan and Planton, 1989, ECMWF, 2014] was utilised:

$$E_{\mathrm{G}} = \frac{\frac{dq_{\mathrm{sat}}}{dT}(R_{\mathrm{n}} - G) + \frac{\rho c_{\mathrm{p}}}{r_{\mathrm{a}}}(q_{\mathrm{sat}}(T) - q_{\mathrm{s}})}{\frac{dq_{\mathrm{sat}}}{dT} + \frac{c_{\mathrm{p}}}{L_{\mathrm{v}}}(1 + \frac{r_{\mathrm{s}}}{r_{\mathrm{a}}})} \tag{10}$$

where $\frac{dq_{\mathrm{sat}}}{dT}$ is the slope of the saturation specific humidity, R_{n} is the net radiation. The aerodynamic resistance r_{a} is obtained in the same way as all the other aerodynamic resistances as described in Masson [2000]. The resistance of the vegetation r_{s} is parameterised as:

$$r_{\mathrm{s}} = \frac{r_{\mathrm{s,min}}}{LAI} f_1(S_{\mathrm{G}}) f_2(W_{\mathrm{G}}) f_3(T_{\mathrm{s}}), \tag{11}$$

$$f_1(S_{\mathrm{G}}) = \min\left(1, \frac{0.004 S_{\mathrm{G}} + 0.05}{0.81(0.004 S_{\mathrm{G}} + 1)}\right)^{-1}, \tag{12}$$

$$f_2(W_{\mathrm{G}}) = \frac{W_{\mathrm{fc}} - W_{\mathrm{wilt}}}{W_{\mathrm{G}} - W_{\mathrm{wilt}}}, \tag{13}$$

$$f_3(T_{\mathrm{s}}) = \frac{1}{1 - 0.0016(T_{\mathrm{s}} - 298)^2}. \tag{14}$$

where LAI is the Leaf Area Index, W_{wilt} is the volumetric soil moisture at wilting point and W_{fc} is the volumetric soil moisture at field capacity.

3. Results

3.1. Steady state

In this section the modified TEB (MTEB) is used to study the effect of green roofs on the local microclimate. Of particular interest is the relationship between air temperature (T) and latent heat flux (E), since the latter can be directly influenced by increasing the area of green roofs or by additional watering of the plants. We study four steady state base scenarios with different geometries and climates described in Table 1. All base scenarios represent summer conditions, with no open water available for evaporation. Hot scenarios (H) are in an environment with high atmospheric temperature (32°C) and solar radiation ($520\mathrm{Wm^{-2}}$), cool (C) scenarios have lower temperature (22°C) and radiation ($480\mathrm{Wm^{-2}}$). The narrow (N) canyon geometry has a street width of 12m and building width of 26m. The wide (W) geometry features 20m wide roads and buildings.

For all cases external forcings, i.e. the incoming solar radiation and atmospheric temperature, were held constant during the simulation, thus given enough time the

Table 1. Scenario parameters.

Case	S [$\mathrm{Wm^{-2}}$]	T_{atm} [°C]	h [m]	b [m]	l [m]
CN	480	22	20	26	12
CW	480	22	20	20	20
HN	520	32	20	26	12
HW	520	32	20	20	20

system attains a steady state. Therefore, the values for S and T_{atm} in Table 1 must be interpreted as daytime means. In reality, urban climate never reaches a steady state and the diurnal cycle plays an important role. Nevertheless, the steady state results will prove to be representative also for cities with a diurnal cycle as will be shown in Section 3.2.

The wind velocity at 48m was $3\mathrm{ms^{-1}}$ and the longwave forcing was modelled as in Swinbank [1963] and is a function of atmospheric temperature. The albedo of the green roof was kept identical to the conventional roof to isolate the effect of evaporative cooling. For each base scenario a series of simulations with combinations of different surface air layer thickness, green roof fraction and varying soil moisture content was carried out and analysed. To define the surface layer thickness the forcing height of the atmosphere was set to 48m, 150m or 300m resulting in a thickness d_{s} of 28m, 130m and 280m, respectively. The fraction of roof covered by vegetation (f_{G}) was varied between 0% and 100% of b in 25% intervals. Soil moisture content W_{G} took one of the following values between wilting point and field capacity in [$\mathrm{kgm^{-2}}$]: $[56, 58, 60, 62, 65, 65.5, 66, 69, 74, 80, 88, 99, 103]$. By varying the soil moisture content the latent heat flux can be influenced while not directly affecting any of the other fluxes. For a soil moisture content at the wilting point or below no evaporation takes place, while the maximum evaporation is reached at field capacity. In all the simulations no runoff was assumed and W_{G} was held constant by supplying water (f_{W}) equal to the evaporation rate (E_{G}). The additional water supply essentially is a forcing on the system, which allows for a steady state to be attained. Thus, (9) simplifies to

$$0 = f_W - E_G, \tag{15}$$

Figure 2a shows the influence of the surface layer thickness on the surface layer temperature ΔT_{s} for the four base scenarios for a green roof fraction of 50% and soil moisture content of $65\mathrm{kgm^{-2}}$. We find that in general the effect on ΔT_{s} is very weak and the curves flatten for increasing layer thickness. A thicker surface layer leads to slightly higher temperatures. This is the result of the resistances depending on the surface layer thickness. The resistance between the surface layer and the atmosphere r_s depends more strongly on the thickness than the resistance between the surface layer and the roof r_R. Thus a thicker layer reduces the flux between the surface layer and the atmosphere more than the flux between the roof and the surface layer.

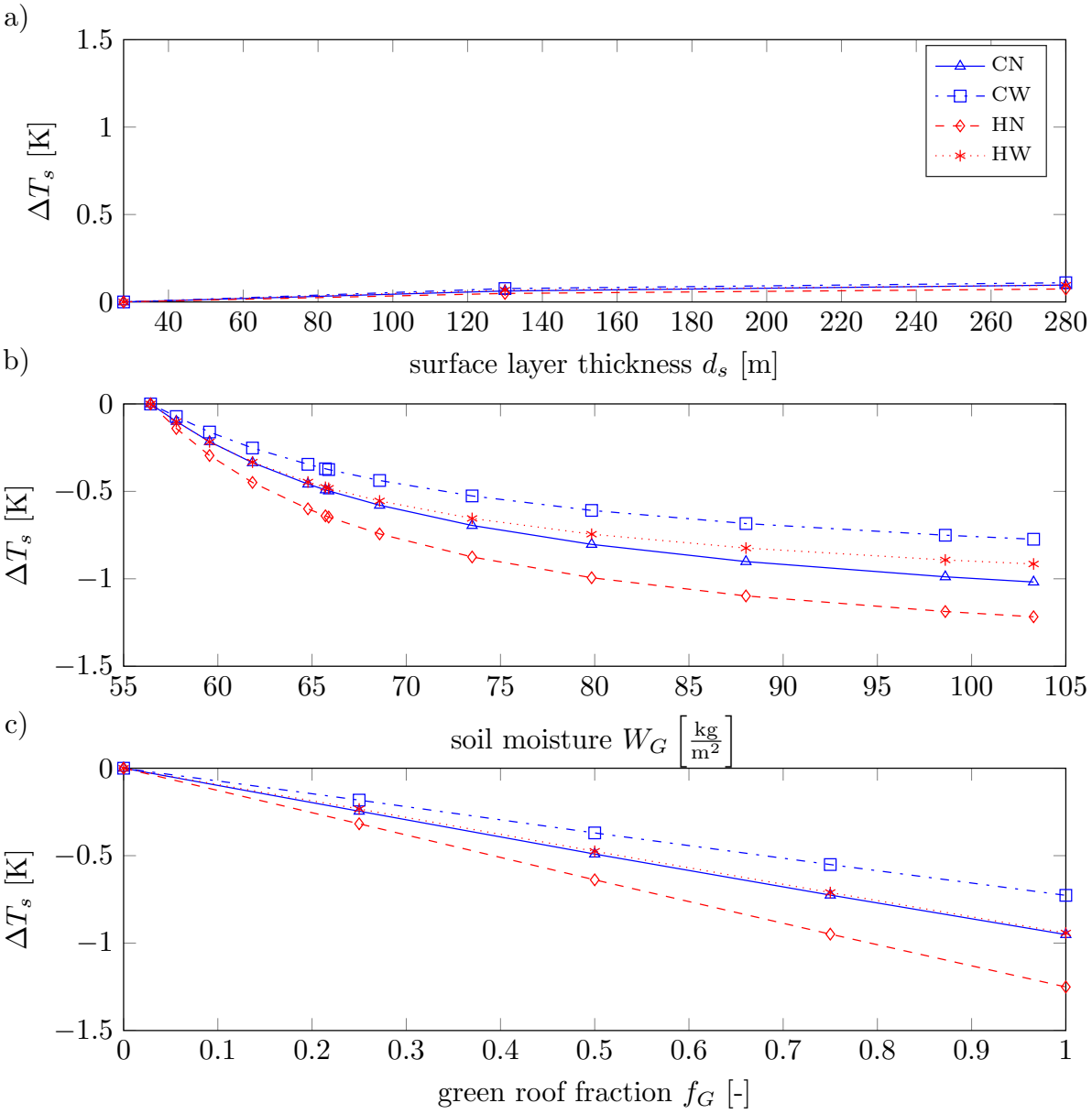

Figure 2. (a) Change of surface layer temperature (ΔT_s) depending on surface layer thickness d_s, (b) soil moisture content W_G and (c) green roof fraction f_G.

Figure 2b shows the change in surface layer temperature depending on the soil moisture content. The surface layer thickness is 130m and the green roof fraction is 50%. We can see that the temperature reduction at the wilting point is 0 since no evaporation occurs. Increasing soil moisture leads to more cooling, but with a decreasing rate. The geometry with narrow roads also has wider buildings as can be seen in Table 1; the same green roof fraction therefore corresponds to a larger vegetated area. The cases CN and HN thus show a stronger temperature reduction for a given soil moisture content. Temperature reduction is also larger in a hotter climate.

Figure 2c shows the change in surface layer temperature depending on the fraction of

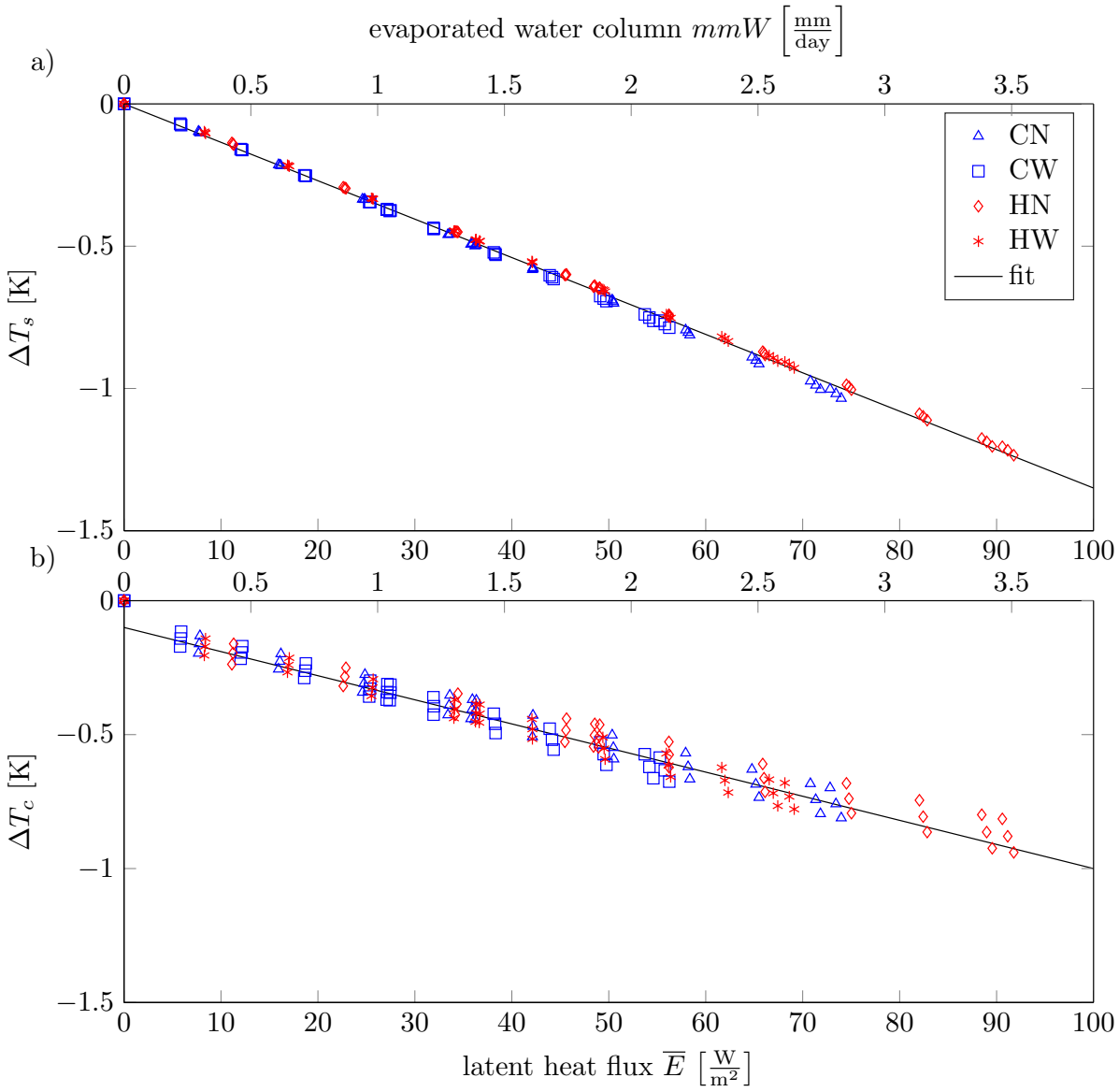

Figure 3. (a) Change of the surface layer air temperature and (b) canyon temperature depending on latent heat flux from vegetated green roofs. Daily evaporated water column corresponding to the latent heat flux on top x-axis.

roofs covered with vegetation. The surface layer thickness is 130m and the soil moisture content was 65kgm^{-2}. We observe a linear relationship between temperature reduction and green roof fraction. Again, hotter conditions lead to a stronger temperature reduction for a given green roof fraction and the geometries with narrower streets offer more roof area, leading to more cooling. These two effects coincidentally lead to an almost identical graph for the HW and CN case.

By plotting surface layer air temperature reduction against the average latent heat flux it is possible to capture all effects shown in Figure 2 in a single plot. Here the latent heat flux is averaged over the entire horizontal area to remove the effect of the different

green roof fractions and roof sizes, i.e.

$$\overline{E} = a_{\mathrm{G}} E_{\mathrm{G}}. \tag{16}$$

Figure 3a shows a collapse of all the data on a single line of the form

$$\Delta T_{\mathrm{s}} = e_{\mathrm{E}} \cdot \Delta \overline{E}, \tag{17}$$

where the gradient e_{E} is the evaporative cooling potential with

$$e_{\mathrm{E}} = -0.014 \mathrm{Km}^2\mathrm{W}^{-1} \tag{18}$$

for all scenarios. Alternatively, the the relationship can be expressed as

$$\Delta T_{\mathrm{s}} = e_{\mathrm{W}} \cdot mmW \tag{19}$$

where mmW is the daily evaporated water column,

$$mmW = \frac{\overline{E}}{L_{\mathrm{v}} \rho_w} \frac{86400\mathrm{s}}{\mathrm{day}}, \tag{20}$$

with the density of water $\rho_w = 1\mathrm{kgdm}^{-3}$, which results in a gradient

$$e_{\mathrm{W}} = -0.35 \mathrm{Kday\,mm}^{-1}. \tag{21}$$

In this form the cooling potential can be better related to the available precipitation. For the remainder of this paper e will always be expressed as e_E in SI units. A previous study by Li et al. [2014] found a comparable relationship between daily mean near surface temperatures and domain average daily mean latent heat flux of -0.018$\mathrm{Km}^2\mathrm{W}^{-1}$ and for daily maximum near surface temperatures -0.022$\mathrm{Km}^2\mathrm{W}^{-1}$ by using the mesoscale atmospheric model WRF-PUCM to study the impact of green roofs on the Baltimore-Washington metropolitan area. Equation (17) allows us to assess the maximal cooling we can achieve with the available precipitation for the given climate or we can estimate the effect additional watering would have on green roof performance, with an upper limit given by green roof area and climate.

Figure 3b shows the temperature reduction inside the canyon. The slope is somewhat smaller at -0.01$\mathrm{Km}^2\mathrm{W}^{-1}$. This is expected since green roofs only interact with the canyon via the surface layer and not directly. Since the resistance between canyon and surface layer depends on the surface layer thickness, the corresponding three cases can clearly be distinguished. We can also observe a deviation from the linear behaviour for very small latent heat fluxes. Due to the indirect interaction of the canyon and the green roof we will continue to focus on surface layer temperature.

3.2. Diurnal cycle

We compare the steady state results to an unsteady case with an idealised diurnal atmospheric temperature and radiation cycles. The forcing corresponds to the HW case with a surface layer thickness of 300m and a green roof fraction of 50%. Daily shortwave radiation is prescribed as $S = S_0 \cdot \max(\sin(\frac{2\pi(t-4\mathrm{h})}{32\mathrm{h}}), 0)$, truncated and repeated after 24h leading to 16h daylight per day. Radiation was set to zero during night time resulting

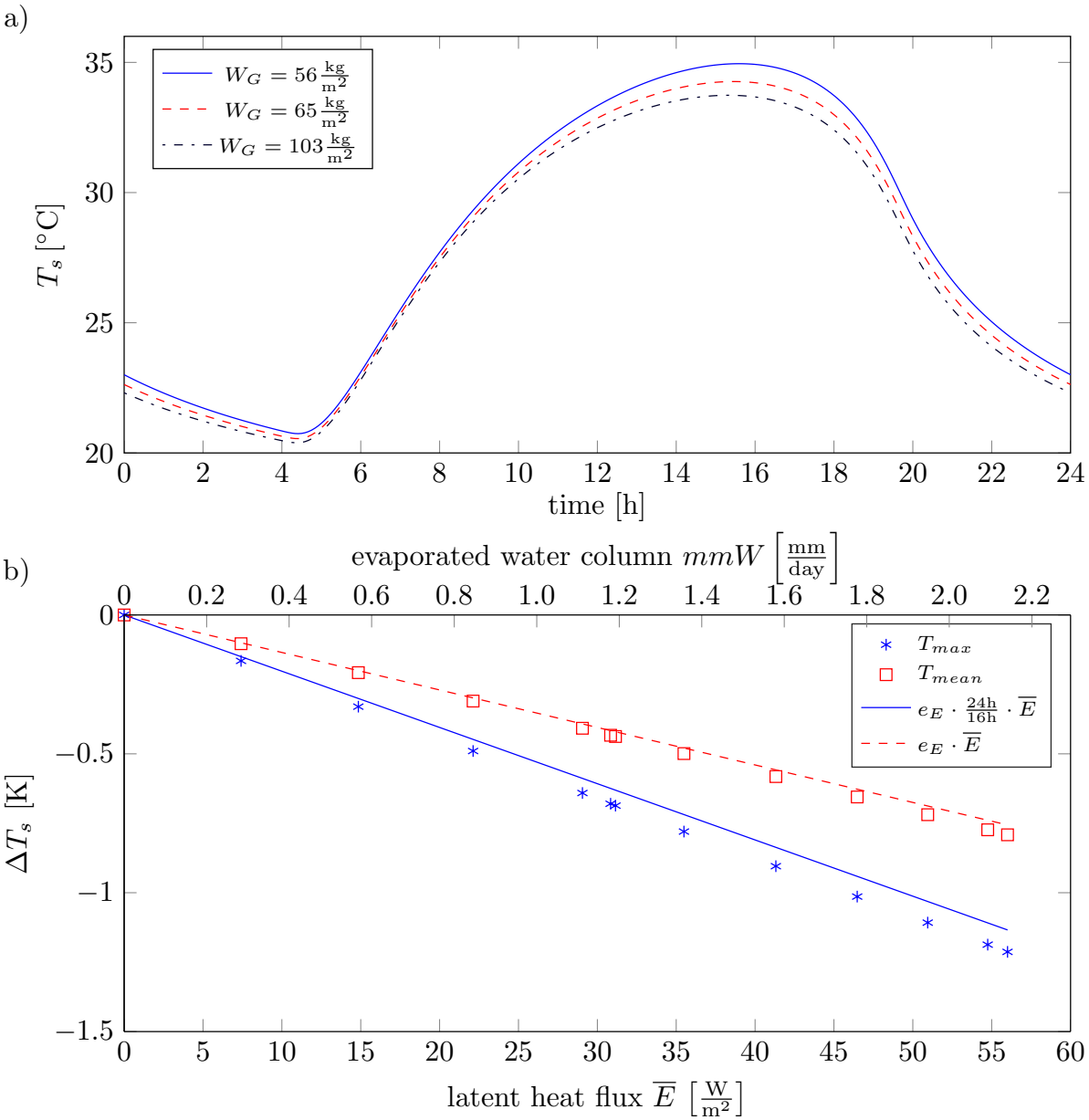

Figure 4. (a) Diurnal cycle of surface layer temperature for the HW case for three different soil moisture contents and (b) reduction of daily mean and maximum temperature due to latent heat flux from green roofs (bottom).

in a daily mean of 520Wm^{-2}. The atmospheric temperature followed the same profile, with constant 293K during the night and a daytime mean of 305K. The resulting surface layer temperatures are shown in the figure 4a.

By changing the soil moisture content we can reproduce figure 3 for daily mean temperatures and maximum temperatures. The daily mean temperatures are the average over the entire day and the maximum temperatures are the peak surface layer temperatures that occur around 16:00 in the afternoon. Figure 4b reveals a linear behaviour for both mean and maximum temperatures even under unsteady conditions

and confirms the assumption that the effect on mean temperature -0.014Km^{2}W^{-1} is lower than on maximum temperatures -0.021Km^{2}W^{-1}. Note that the effect on mean temperature in the unsteady case is very close to the findings for a steady state (shown as dashed line), thereby confirming representativeness of simplified steady state assumption. While the choice of daily mean latent heat flux or evaporated water column is convenient for comparison with available precipitation it is not ideal to examine temperature extremes. The temperature maximum is a daytime phenomenon (under hot summer conditions) and in this idealised case the day is 16h (t_d) and night 8h long. Since evapotranspiration at night is minimal, mean daytime evaporation is approximately 24h/16h$\cdot\overline{E}$ and we indeed find

$$\Delta T_{\mathrm{s,max}} \approx e_\mathrm{E} \cdot \frac{24h}{t_\mathrm{d}} \cdot \Delta\overline{E}. \tag{22}$$

3.3. Methods of water supply

In sections 3.1 and 3.2 the soil moisture W_G was held constant by supplying water at a rate f_W equal to the evaporation rate E_G during all the simulations, which is a necessary condition to reach a steady state. In this section, we will show that our results do not depend sensitively on the method of water supply. In particular, we carry out additional simulations without constant soil moisture, but various methods of water supply, namely:

(i) No water supply, soil moisture slowly depleting
(ii) Using a time series of actual rainfall as forcing
(iii) Watering for 30min in the morning
(iv) Constant watering throughout the day, drip irrigation.

The time series of the water supply can be seen in figure 5a. The rainfall data has been collected during three summer days of the CAPITOUL experiment in Toulouse, France [Masson et al., 2008] and amounts to 10.4mm over the three days. The total water supplied by constant irrigation is 6.5mm and by morning irrigation 4.9mm over three days, respectively. The geometry and diurnal forcing used were identical to the unsteady case in section 3.2 and different evaporation rates were achieved by varying initial soil moisture.

From the results shown in figure 5b it is clear that the slope e_E is robust and does not significantly depend on the chosen supply method. The "mean" quantities are averaged over the third day. $\overline{E}$ and $\Delta T_{s,mean}$ are thus the 1-day averages of the differences between a scenario with evaporation and one without. The temperature reduction $\Delta T_{s,max}$ is the difference between the daily maximum temperature of scenarios with and without evaporation during the third day. It is important to consider that when plotting ΔT vs E, excess water does not show up in the graph, since it runs off and does not evaporate. The water supply to green roofs in reality would thus need to be larger than the evaporated water column in the paper suggests, since runoff can usually not

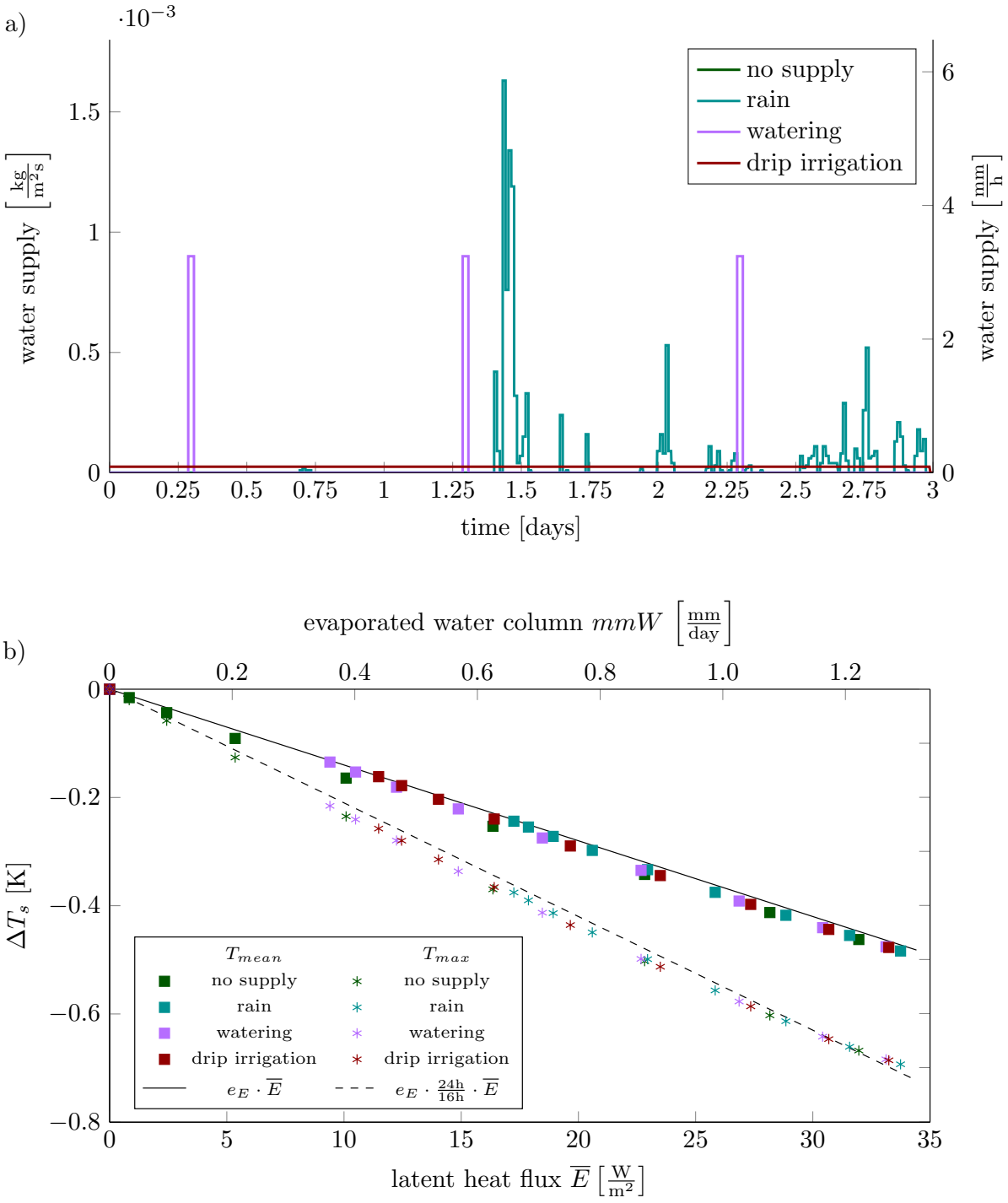

Figure 5. a) Time series of the supplied water for each method of water supply and b) resulting change of daily mean and maxima surface layer air temperatures depending on latent heat flux from vegetated green roofs for each method. Daily evaporated water column corresponding to the latent heat flux on top x-axis.

be completely avoided. It is thus recommended to chose drip irrigation to avoid runoff of excess water and achieve a larger cooling.

4. A simple estimate of the evaporative cooling potential

To better understand what processes influence the evaporative cooling potential e and to estimate the value without having to solve the set of differential equations numerically, we derive an algebraic expression for e. The MTEB model is a set of ODEs describing the evolution of heat and water reservoirs over time. Every differential equation is based on a flux balance. The exchange processes between the reservoirs and between the reservoirs and the atmosphere are described by various functions depending on the current state of the system, $\boldsymbol{x} = [T_R, T_w, T_r, q_s, T_s, T_G, W_G]^T$. A very general way to express the MTEB model is then

$$C\frac{d\boldsymbol{x}}{dt} = \boldsymbol{g}(\boldsymbol{x}) + \boldsymbol{f} \tag{23}$$

where C is a diagonal matrix containing the heat capacities. The external forcing on the system, notably the solar short-wave radiation and water supply (f_W) is given by

$$\boldsymbol{f} = [S_R, S_w, S_r, 0, 0, S_G, f_W]^T . \tag{24}$$

The 7×1 column vector $\boldsymbol{g} = (g_1(\boldsymbol{x}), g_2(\boldsymbol{x}), ...)$ contains the energy and water balances (equations (2), (3), (7), (8), (9)) and defines the evolution of x_i with time. To analyse the reaction of this system to a perturbation from a reference state $\boldsymbol{x}_0$ we perform a multivariate Taylor series expansion with result

$$C\frac{d\boldsymbol{x}}{dt} = \boldsymbol{g}(\boldsymbol{x_o}) + J\boldsymbol{\epsilon} + \boldsymbol{f} + \mathrm{O}\big(\epsilon^2\big), \tag{25}$$

where $\boldsymbol{\epsilon} = \boldsymbol{x} - \boldsymbol{x_o}$ is the deviation from the reference state and $J_{ij} = \frac{\partial g_i}{\partial x_j}|_{\boldsymbol{x}_0}$ is the Jacobian given by

$$J = \begin{bmatrix} J_{11} & 0 & 0 & 0 & J_{15} & 0 & 0 \\ 0 & J_{22} & J_{23} & 0 & J_{25} & 0 & 0 \\ 0 & J_{32} & J_{33} & 0 & J_{35} & 0 & 0 \\ 0 & 0 & 0 & J_{44} & J_{45} & J_{46} & J_{47} \\ J_{51} & J_{52} & J_{53} & 0 & J_{55} & J_{56} & 0 \\ 0 & 0 & 0 & J_{64} & J_{65} & J_{66} & J_{67} \\ 0 & 0 & 0 & J_{74} & J_{75} & J_{76} & J_{77} \end{bmatrix}, \tag{26}$$

with e.g. $J_{11} = \frac{\partial g_1}{\partial T_R}$ and $g_1(T_R) = L_R(T_R) - H_R(T_R) - G_R(T_R)$ (from (2)). Thus the change of the roof temperature with time depends on the roof temperature itself via functions describing the longwave radiation, sensible heat flux and ground heat flux. To keep the Taylor series tractable we ignore the dependence of resistances upon $\boldsymbol{x}$.

We are interested in a change in forcing $\boldsymbol{f} = \boldsymbol{f_o} + \boldsymbol{f}_\delta$, where $\boldsymbol{f}_\delta = [0, 0, 0, 0, 0, 0, \Delta f_W]^T$ contains a change in water supply (in Wm^{-2}). Here, $\boldsymbol{f} = \boldsymbol{f_o}$ corresponds to the steady state forcing in the reference state for which $\frac{d\boldsymbol{x}}{dt} = 0$ and

$\boldsymbol{\epsilon} = 0$; hence $\boldsymbol{g}(\boldsymbol{x_o}) = -\boldsymbol{f_o}$, implying that the fluxes in the system balance the external forcing in the steady state. Thus, it follows from (25) that the modified steady state of the system is governed by

$$\boldsymbol{\epsilon} = -J^{-1}\boldsymbol{f}_\delta. \tag{27}$$

Written out and making use of the fact that $\boldsymbol{f}_\delta$ contains zeros except for the last entry, this relation reads

$$\begin{bmatrix} \Delta T_R \\ \Delta T_w \\ \Delta T_r \\ \Delta q_s \\ \Delta T_s \\ \Delta T_G \\ \Delta W_G \end{bmatrix} = - \begin{bmatrix} J^{-1}_{17} \\ J^{-1}_{27} \\ J^{-1}_{37} \\ J^{-1}_{47} \\ J^{-1}_{57} \\ J^{-1}_{67} \\ J^{-1}_{77} \end{bmatrix} \Delta f_W. \tag{28}$$

The evaporative cooling potential, e, which links ΔT_s to the domain-averaged latent heat flux $\overline{E} = a_G E_G$ is given by

$$e_E = -J^{-1}_{57} a_G^{-1}, \tag{29}$$

making use of (15).

The Jacobian J can be obtained readily by making use of symbolic mathematics software such as MAPLE, after which J can be evaluated numerically and then inverted for any reference state. This works for any UEB, as long as the functions $\boldsymbol{g}$ and their derivatives are known. For the HW scenario with 50% green roof fraction and 28m surface layer thickness the result is

$$J = \begin{bmatrix} -27.34 & 0 & 0 & 0 & 17.76 & 0 & 0 \\ 0 & -14.1 & 5.45 & 0 & 4.47 & 0 & 0 \\ 0 & 12.9 & -19.3 & 0 & 4.47 & 0 & 0 \\ 0 & 0 & 0 & -96450 & 1.13 & -0.69 & 2.07 \\ 4.44 & 4.47 & 2.23 & 0 & -58.0 & 4.44 & 0 \\ 0 & 0 & 0 & 3122 & 13.22 & -24.3 & -8.30 \\ 0 & 0 & 0 & 3122 & -4.54 & 2.74 & -8.30 \end{bmatrix} \tag{30}$$

and

$$J^{-1} = \begin{bmatrix} -38.7 & -7.7 & -3.7 & 0.0 & -13 & -2.2 & 2.2 \\ -1.8 & -102 & -30 & 0.0 & -11 & -1.9 & 1.9 \\ -2.5 & -71 & -73.3 & 0.0 & -12.4 & -2 & 2 \\ 0.0 & 0.0 & 0.0 & -0.01 & 0.0 & 0.0 & -0.0 \\ -3.4 & -12 & -5.7 & 0.0 & -20 & -3.4 & 3.4 \\ -2.2 & -7.8 & -3.8 & 0.0 & -13.6 & -3.9 & 3.9 \\ 1 & 3.9 & 1.9 & -4 & 6.8 & -11 & -11 \end{bmatrix} \times 10^{-3}. \tag{31}$$

In this case $-J^{-1}_{57} = -0.0034 \mathrm{Km^2W^{-1}}$. With the given green roof fraction and geometry the green roof makes up 25% of the entire area, and thus $e_E = -J^{-1}_{57}/0.25 =$

$-0.0136\mathrm{Km}^2\mathrm{W}^{-1}$, which is very close to the value of -0.0135 we obtain by solving the ODE numerically.

The approach above, although correct, is neither amenable to hand calculations, nor does it provide insight into physical processes. We thus simplify (26) further by assuming that feedback processes can be neglected for small $\boldsymbol{\epsilon}$. Without feedback mechanism it is possible to reduce the number of equations required to determine e_E. A forcing on the soil moisture content W_G will initially only affect E_G, whose derivatives appear in J_{47}, J_{67} and J_{77}. We can thus disregard the conventional roof temperature $T_R \Longrightarrow J_{1,\star}$, $T_w \Longrightarrow J_{2,\star}$ and $T_r \Longrightarrow J_{3,\star}$ entirely. Since we are interested in surface layer temperature and T_s does not directly depend on q_s we can also ignore $J_{4,\star}$. Furthermore, without feedback processes only the upper triangular part of this reduced matrix is important. The simplified Jacobian is then given by

$$J_s = \begin{bmatrix} J_{55} & J_{56} & 0 \\ 0 & J_{66} & J_{67} \\ 0 & 0 & J_{77} \end{bmatrix} \tag{32}$$

and the simplified system is

$$\boldsymbol{\epsilon}_s = -\begin{bmatrix} \Delta T_s \\ \Delta T_G \\ \Delta W_G \end{bmatrix} = J_s^{-1} \begin{bmatrix} 0 \\ 0 \\ \Delta f_W \end{bmatrix}. \tag{33}$$

Specific to the current problem is that J_{67} and J_{77} are identical by definition, as they both describe the same physical process, namely the evaporation from the green roof which shows up both in the water and in the energy balance. Making use of of this inverting J_s yields an estimate for e_E given by

$$e_{Es} = -a_G^{-1}\frac{J_{56}}{J_{55}J_{66}} = -a_G^{-1}\frac{\frac{\partial g_5}{\partial T_G}}{\frac{\partial g_5}{\partial T_s}\frac{\partial g_6}{\partial T_G}}. \tag{34}$$

We can verify that (34) corresponds to e_{Es} by using that under the simplified conditions $e_{Es} = a_G^{-1}\frac{-J_{56}}{J_{55}}\frac{1}{J_{66}} = a_G^{-1}\frac{\Delta T_s}{\Delta T_G}\frac{\Delta T_G}{a_G^{-1}\Delta \overline{E}}$, which is indeed the definition of e_E given by (17). In (34) g_5 describes the evolution of surface layer temperature with time and g_6 describes the evolution of the green roof temperature. The only term in g_5 depending on the green roof temperature is the sensible heat flux from the green roof and thus the numerator of (34) consists of a single term. The denominator describes how the temperatures depend on themselves and contains all the terms from the energy budgets Eq. (7) and (2), without the shortwave radiation. Thus,

$$e_{Es} = \frac{-a_G^{-1}\frac{\partial H_G}{\partial T_G}}{\left(-\frac{\partial H_s}{\partial T_s} + \frac{\partial H_R}{\partial T_s} + \frac{\partial H_c}{\partial T_s} + \frac{\partial H_G}{\partial T_s}\right)\left(\frac{\partial L_G}{\partial T_G} - \frac{\partial H_G}{\partial T_G} - \frac{\partial G_G}{\partial T_G} - \frac{\partial E_G}{\partial T_G}\right)}. \tag{35}$$

Most terms in (35) are simple to evaluate using (4) for sensible and (6) for ground heat flux. Longwave radiation follows the Stefan-Boltzman law. Only the term $\frac{\partial E_G}{\partial T_G}$ depends

on the model choice and is a lengthy algebraic expression. Specifically, e_{Es} takes the form

$$e_{Es} = \frac{-1}{a_G(-4\epsilon\sigma T_{G0}^3 - \frac{\rho_a c_p}{r_R} - \frac{\lambda_R}{d_R} - \frac{\partial E_G}{\partial T_G})} \frac{R}{r_R}, \tag{36}$$

where R can be interpreted as a net parallel resistance associated with the surface layer and is given by

$$\frac{1}{R} = \left(-\frac{1}{r_s} + \frac{a_R}{r_R} + \frac{a_c}{r_R} \left(\frac{1}{\frac{3r_R}{r_c} + 1} - 1 \right) + \frac{a_G}{r_R} \right). \tag{37}$$

The dominant term in (36) was found to be r_s^{-1} in our scenarios. This implies that a vastly different stability between the surface layer and the atmosphere could lead to significant changes in e. Yet, the surface layer is usually convective and resistances are low during daytime urban heat island conditions, limiting the actual effect of r_s. Evaluating e_{Es} for the given reference values for the HW case results in

$$e_{Es} = -0.0126 \frac{\mathrm{Km}^2}{\mathrm{W}}. \tag{38}$$

This simplified expression (35) produces a reasonably good estimate for e compared to the full MTEB model and can be used for any other chosen formulations of energy fluxes in other UEB models or other tools to assess the urban climate. The evaporative cooling potential can thus be derived without having to resort to complicated modelling.

5. Concluding remarks

We performed a study to quantify to what extent green roofs can help to mitigate the urban heat island effect. By exploring the properties of a modified urban energy balance model, we found a robust linear relationship between average latent heat flux $\overline{E}$ and mean surface layer temperature reduction ΔT_s. The gradient of this curve, which we refer to as the evaporative cooling potential e_E is approximately -0.014 $\mathrm{Km}^2\mathrm{W}^{-1}$ for steady state conditions, which is a reasonable representation for daily average temperature reduction (17) and is in good agreement with more sophisticated modeling approaches [Li et al., 2014]. We also observe that e_E is independent of the method by which water is supplied to the green roofs. In terms of the average daily water evaporation, e can be expressed as $e_W \approx -0.35\,\mathrm{Kdaymm}^{-1}$. More relevant for the urban heat island effect is the temperature reduction for daily maximum temperatures, which could be approximated by simply dividing by the fraction of daytime hours per day (22). We explored the underlying physical reason behind this linear trend using Taylor series approximations, and derived a relatively simple algebraic relation (35) that estimates e within a 10% margin of error. We find that e does depend on the surface layer resistance r_s, since the dominant term in (36) is r_s^{-1}. Emphasis should thus be placed on the parameterisation of r_s.

The evaporative cooling potential is a useful tool for city planners to get a rough first order estimate of how much cooling green roofs can provide. Indeed, we can use

e_W to estimate the possible cooling from green roofs in a city by comparing the daily evaporated water column to the mean daily precipitation in that city. For example London, with a mean summer precipitation of about 1.5mmday^{-1}, can achieve an average surface layer temperature reduction of 0.4K if all the water above urban areas could be retained and evaporated. Without additional watering the outdoor cooling effect of green roofs in London will thus be rather small. However, the effect on daily maximum temperatures is larger and during very hot days small temperature reductions can have a significant influence on health [Kovats and Hajat, 2008, Luber and McGeehin, 2008].

The small amount of precipitation generally available during hot periods in mid-latitudes indicates that neither the precise climate nor urban geometry are expected to be the limiting factors in the cooling potential of green roofs and e is therefore expected to be quite universal. Indeed, water availability is the main limiting factor. Increasing the area of green roofs to retain more water is a possible way to achieve more cooling. Yet, when capturing precipitation by other means (e.g. rain gutters) and using it to water green roofs, relatively small green roof fractions can achieve the same amount of cooling.

Most of human activities take place inside the urban canyon and it can thus be argued that the effect of green roofs on canyon air temperatures is of greater significance than on surface air layer. Green roofs appear to be an inefficient tool to reduce canyon air temperature directly. Other blue-green infrastructure like green walls may have a larger temperature impact. However, anthropogenic heat sources have not been considered in this paper. Indeed, HVAC (heating, ventilation and air conditioning) units are often installed on walls and produce large amounts of heat inside the canyons. Green roofs lead to cooler roof temperatures, and thus reduce the heat flux into the indoor environment and could therefore indirectly influence the canyon air temperatures significantly. There are further limitations to this study that deserve detailed investigation, notably the effect of heterogeneous geometry and plant albedo. Further research is also needed to assess other green infrastructure strategies like e.g. green walls, swales and parks.

Acknowledgements

The authors wish to acknowledge the support of the European Institute of Technology, Climate KIC Innovation project Blue Green Dream. We would like to thank Matteo Malacarne for working on an early prototype of MTEB as part of his final year MEng project and we sincerely appreciate the valuable input of Dr. Ana Mijic and our discussions with her.

References

M. J. Best, M. Pryor, D. B. Clark, and G. G. Rooney. The Joint UK Land Environment Simulator (JULES), model description - Part 1: Energy and water fluxes. *Geoscientific Model Development*, 4:677 – 699, 2011. doi: 10.5194/gmd-4-677-2011.

H.F. Castleton, V. Stovin, S.B.M. Beck, and J.B. Davison. Green roofs; building energy savings and the potential for retrofit. *Energy and Buildings*, 42(10):1582–1591, October 2010. ISSN 0378-7788. URL `http://www.sciencedirect.com/science/article/pii/S0378778810001453`.

D. B. Clark, L. M. Mercado, S. Sitch, C. D. Jones, N. Gedney, M. J. Best, M. Pryor, G. G. Rooney, R. L. H. Essery, E. Blyth, O. Boucher, R. J. Harding, C. Huntingford, and P. M. Cox. The Joint UK Land Environment Simulator (JULES), model description - Part 2: Carbon fluxes and vegetation dynamics. *Geosci. Model Dev.*, 4(3):701–722, September 2011. ISSN 1991-9603. URL `http://www.geosci-model-dev.net/4/701/2011/`.

ECMWF. IFS Documentation. Technical report, ECMWF, 2014. URL `https://software.ecmwf.int/wiki/display/IFS/CY41R1+Official+IFS+Documentation`.

Matei Georgescu, Philip E. Morefield, Britta G. Bierwagen, and Christopher P. Weaver. Urban adaptation can roll back warming of emerging megapolitan regions. *Proceedings of the National Academy of Sciences*, 111(8):2909–2914, February 2014.

Kristin L. Getter and D. Bradley Rowe. The role of extensive green roofs in sustainable development. *HortScience*, 41(5):1276–1285, 2006.

C. S. B. Grimmond, M. Blackett, M. J. Best, J. Barlow, J.J. Baik, S. E. Belcher, S. I. Bohnenstengel, I. Calmet, F. Chen, A. Dandou, K. Fortuniak, M. L. Gouvea, R. Hamdi, M. Hendry, T. Kawai, Y. Kawamoto, H. Kondo, E. S. Krayenhoff, S-H. Lee, T. Lordian, A. Martilli, V. Masson, S. Miao, K. Oleson, G. Pigeon, A. Porson, Y-H. Ryu, F. Salamanca, L. Shashua-Bar, G-J. Steeneveld, M. Tombrou, J. Voogt, D. Young, and N. Zhang. The International Urban Energy Balance Models Comparison Project: First Results from Phase 1. *J. Appl. Meteor. Climatol.*, page 12681292, 2010. ISSN 49.

Christof Gromke, Bert Blocken, Wendy Janssen, Bart Merema, Twan van Hooff, and Harry Timmermans. CFD analysis of transpirational cooling by vegetation: Case study for specific meteorological conditions during a heat wave in Arnhem, Netherlands. *Building and Environment*, 83:11–26, January 2015. ISSN 0360-1323. URL `http://www.sciencedirect.com/science/article/pii/S0360132314001267`.

IPCC. Climate Change 2014: Impacts, Adaptation, and Vulnerability. Part B: Regional Aspects. Contribution of Working Group II to the Fifth Assessment Report of the Intergovernmental Panel on Climate Change. Technical report, Intergovernmental Panel on Climate Change, 2014.

P. G. Jarvis. The interpretation of the variations in leaf water potential and stomatal conductance found in canopies in the field. *Philosophical Transactions of the Royal Society of London B: Biological Sciences*, 273(927):593–610, February 1976. URL http://rstb.royalsocietypublishing.org/content/273/927/593.abstract.

R. Sari Kovats and Shakoor Hajat. Heat stress and public health: A critical review. *Annu. Rev. Public Health*, 29(1):41–55, March 2008. ISSN 0163-7525. doi: 10.1146/annurev.publhealth.29.020907.090843. URL http://dx.doi.org/10.1146/annurev.publhealth.29.020907.090843.

D. Li, E. Bou-Zeid, and M. Oppenheimer. The effectiveness of cool and green roofs as urban heat island mitigation strategies. *Environ. Res. Lett.*, 055002:16, 2014. ISSN 9.

George Luber and Michael McGeehin. Climate change and extreme heat events. *American Journal of Preventive Medicine*, 35(5):429–435, November 2008. ISSN 0749-3797. URL http://www.sciencedirect.com/science/article/pii/S0749379708006867.

Christopher W. Mackey, Xuhui Lee, and Ronald B. Smith. Remotely sensing the cooling effects of city scale efforts to reduce urban heat island. *Building and Environment*, 49:348–358, March 2012. ISSN 0360-1323. URL http://www.sciencedirect.com/science/article/pii/S0360132311002472.

V Masson. A physically-based scheme for the urban energy budget in atmospheric models. *Boundary-Layer Meteorology*, 94:357–397, 2000. URL http://link.springer.com/article/10.1023/A:1002463829265.

V. Masson, L. Gomes, G. Pigeon, C. Liousse, V. Pont, J.-P. Lagouarde, J. Voogt, J. Salmond, T. R. Oke, J. Hidalgo, D. Legain, O. Garrouste, C. Lac, O. Connan, X. Briottet, S. Lachrade, and P. Tulet. The canopy and aerosol particles interactions in toulouse urban layer (capitoul) experiment. *Meteorology and Atmospheric Physics*, 102(3-4):135–157–, 2008. ISSN 0177-7971. URL http://dx.doi.org/10.1007/s00703-008-0289-4.

Janusz Niemczynowicz. Urban hydrology and water management - present and future challenges. *Urban Water*, 1(1):1–14, March 1999. ISSN 1462-0758. URL http://www.sciencedirect.com/science/article/pii/S1462075899000096.

J. Noilhan and S. Planton. A simple parameterization of land surface processes for meteorological models. *Mon. Wea. Rev.*, 117(3):536–549, March 1989. ISSN 0027-0644. doi: 10.1175/1520-0493(1989)117⟨0536:ASPOLS⟩2.0.CO;2. URL http://dx.doi.org/10.1175/1520-0493(1989)117<0536:ASPOLS>2.0.CO;2.

Erica Oberndorfer, Jeremy Lundholm, Brad Bass, Reid R Coffman, Hitesh Doshi, Nigel Dunnett, Stuart Gaffin, Manfred Köhler, Karen K Y Liu, and Bradley Rowe. Green Roofs as Urban Ecosystems: Ecological Structures, Functions, and Services. *BioScience*, 57:823–833, 2007. URL http://bioscience.oxfordjournals.org/content/57/10/823.abstract.

T R Oke. Street design and urban canopy layer climate. *Energy and Buildings*, 11:103–113, 1988. ISSN 0378-7788. doi: 10.1016/0378-7788(88)90026-6. URL <GotoISI>://WOS:A1988M778500010.

R. Rojas, L. Feyen, A. Bianchi, and A. Dosio. Assessment of future flood hazard in europe using a large ensemble of bias-corrected regional climate simulations. *Journal of Geophysical Research: Atmospheres*, 117(D17):n/a–n/a, 2012. ISSN 2156-2202. doi: 10.1029/2012JD017461. URL http://dx.doi.org/10.1029/2012JD017461. D17109.

C. Rosenzweig, W. Solecki, P. Romero-Lankao, S. Mehrotra, S. Dhakal, T. Bowman, and S.. Ali Ibrahim. ARC3.2 Summary for City Leaders, 2015.

M. Santamouris. Cooling the cities - a review of reflective and green roof mitigation technologies to fight heat island and improve comfort in urban environments. *Solar Energy*, 103:682–703, May 2014. ISSN 0038-092X. URL http://www.sciencedirect.com/science/article/pii/S0038092X12002447.

Ting Sun, C. S. B. Grimmond, and Guang-Heng Ni. How do green roofs mitigate urban thermal stress under heat waves? *Journal of Geophysical Research: Atmospheres*, 121(10):5320–5335, 2016. ISSN 2169-8996. doi: 10.1002/2016JD024873. URL http://dx.doi.org/10.1002/2016JD024873. 2016JD024873.

W. C. Swinbank. Long-wave radiation from clear skies. *Quarterly Journal of the Royal Meteorological Society*, 89(381):339–348, 1963. ISSN 1477-870X. doi: 10.1002/qj.49708938105. URL http://dx.doi.org/10.1002/qj.49708938105.

UNFPA. State of World Population 2012. Technical report, United Nations Population Fund, 2012.

Jiachuan Yang, Zhi-Hua Wang, Matei Georgescu, Fei Chen, and Mukul Tewari. Assessing the impact of enhanced hydrological processes on urban hydrometeorology with application to two cities in contrasting climates. *Journal of Hydrometeorology*, 17(4):1031–1047, 2016. doi: 10.1175/JHM-D-15-0112.1.